Biophysical Journal Volume 106 June 2014 2417–2425

Direct Visualization of the Action of Triton X-100 on Giant Vesicles of Erythrocyte Membrane Lipids

Bruna R. Casadei,[†] Cleyton C. Domingues,[†] Eneida de Paula,[†] and Karin A. Riske[‡*]

[†]Departamento de Bioquímica, Instituto de Biologia, Universidade Estadual de Campinas, Campinas, Brazil; and [‡]Departamento de Biofísica, Universidade Federal de São Paulo, São Paulo, Brazil

ABSTRACT The raft hypothesis proposes that microdomains enriched in sphingolipids, cholesterol, and specific proteins are transiently formed to accomplish important cellular tasks. Equivocally, detergent-resistant membranes were initially assumed to be identical to membrane rafts, because of similarities between their compositions. In fact, the impact of detergents in membrane organization is still controversial. Here, we use phase contrast and fluorescence microscopy to observe giant unilamellar vesicles (GUVs) made of erythrocyte membrane lipids (erythro-GUVs) when exposed to the detergent Triton X-100 (TX-100). We clearly show that TX-100 has a restructuring action on biomembranes. Contact with TX-100 readily induces domain formation on the previously homogeneous membrane of erythro-GUVs at physiological and room temperatures. The shape and dynamics of the formed domains point to liquid-ordered/liquid-disordered (*Lo*/*Ld*) phase separation, typically found in raft-like ternary lipid mixtures. The *Ld* domains are then separated from the original vesicle and completely solubilized by TX-100. The insoluble vesicle left, in the *Lo* phase, represents around 2/3 of the original vesicle surface at room temperature and decreases to almost 1/2 at physiological temperature. This chain of events could be entirely reproduced with biomimetic GUVs of a simple ternary lipid mixture, 2:1:2 POPC/SM/chol (phosphatidylcholine/sphyngomyelin/cholesterol), showing that this behavior will arise because of fundamental physicochemical properties of simple lipid mixtures. This work provides direct visualization of TX-100-induced domain formation followed by selective (*Ld* phase) solubilization in a model system with a complex biological lipid composition.

INTRODUCTION

Biological membranes are complex and dynamic systems responsible for a variety of cellular activities such as compartmentalization, communication, transport, and energy conversion (1). The raft hypothesis (2) postulates that functional domains rich in sphingolipids, cholesterol, and certain classes of proteins are momentarily assembled to perform crucial roles in several essential cellular processes, such as endocytosis and cell signaling (2,3). The existence of rafts is still controversial, but a large body of evidence gives support to their existence and physiological role (4–9). The importance of the lipid composition in biological membranes became evident from studies in model membranes composed of mimetic lipid mixtures. In a certain composition and temperature range, simple ternary lipid mixtures of unsaturated, long saturated lipids, and cholesterol exhibit macroscopic phase separation between a liquid-disordered (*Ld*) phase—rich in unsaturated lipids—and a liquid-ordered (*Lo*) phase—rich in saturated lipids and cholesterol (10). In particular, observation of giant unilamellar vesicles (GUVs) has proven to be a key approach in determining lateral phase separation in model membranes of different lipid compositions (10–12) and in cellular extracts (6,13,14).

Given the variety and complexity of the composition of biological membranes, a convenient way to separate membrane components and study them individually is via protocols of membrane solubilization with detergents. Such procedure often leaves insoluble fractions, the so-called detergent-resistant membranes (DRMs) (2), which are also rich in raft-like components (15,16). Thus, DRMs were initially assumed to be identical to membrane rafts (17,18). However, DRMs were shown to be highly detergent- and protocol-dependent (15,16,19) and detergent insertion into the membrane can certainly alter and reshape the membrane and lead to nonphysiological conditions (20–22). Detergent extraction of membrane constituents is often performed via standard protocols in which the effect of the detergent on membrane structure is not followed during the solubilization process. Therefore, a deeper understanding of the effects of detergents on biological membranes is still lacking and can certainly help unravel the complex architecture of biological membranes.

The nonionic detergent Triton X-100 (TX-100) has been widely used in protocols of membrane solubilization and extraction of DRMs (21,23). Therefore, various studies have addressed the TX-100-induced solubilization of biological membranes (24,25) as well as of model membranes of diverse composition and in different phases (26–29). The ability of TX-100 to interact and solubilize membranes is strongly modulated by the lipid phase and composition (27,30,31). It has been reported that TX-100 induces *Lo*/*Ld* phase separation in model membranes with preferential solubilization of the *Ld* phase (20,32,33). However, visualization of these effects induced by TX-100 on model systems was achieved only with atomic force

Submitted March 6, 2014, and accepted for publication April 29, 2014.

*Correspondence: kariske@unifesp.br

Editor: Heiko Heerklotz.

0006-3495/14/06/2417/9 $2.00

http://dx.doi.org/10.1016/j.bpj.2014.04.039

microscopy (AFM) of supported lipid bilayers (32,33), which might be influenced by the solid support. Rearrangement of membrane components induced by TX-100 was also observed in biological membranes (21,34). Similarly, unsaturated lipids are preferentially solubilized from biological membranes (21), and TX-100 DRMs were shown to be enriched in sphingolipids and cholesterol (35). Yet, it has been claimed that TX-100 might rather induce coalescence of preexisting nanodomains than formation of new domains from a homogeneous mixture (36).

Here, we use optical microscopy to directly observe the effects of TX-100 on a model system closer to a biological membrane: GUVs made of erythrocyte membrane lipid extract. Erythrocyte plasma membranes have been described in great detail (37) and they are suitable for the study of biological membranes because erythrocytes contain no organelles, making the isolation of their plasma membrane quite simple. In addition, the alterations caused by detergents in dynamic and structural properties of erythrocyte membranes can be monitored by different approaches (8,25,38), making this complex biomembrane a suitable model to explore the effect of detergents on membrane organization. Although GUVs of erythrocyte lipids are still a simplified model of erythrocyte membranes, because proteins are absent and lipid asymmetry is lost, they preserve the complex lipid composition and can reveal lipid-dependent behavior of erythrocytes in a controlled situation. For comparison, GUVs made of the biomimetic ternary composition palmitoyl oleoyl phosphatidylcholine (POPC), egg sphingomyelin (SM), and cholesterol are also investigated. Previously, the solubilization process of POPC by TX-100 has revealed that TX-100 initially inserts into the bilayer, causing a considerable increase in vesicle surface area, followed by opening of holes and complete solubilization (28). Here, we show that TX-100 first induces *Lo*/*Ld* phase separation followed by solubilization of the *Ld* phase only. Interestingly, the *Ld* domains that were first separated from the insoluble *Lo* vesicle, could even form separated vesicles, and were only then completely solubilized by TX-100. The fraction of insoluble vesicle surface area is quantified at room and physiological temperatures and a composition for the insoluble membrane is proposed. The behavior obtained for GUVs made of erythrocyte lipids could be well reproduced with a simple ternary lipid mixture, showing that this is a universal effect of TX-100 on lipid membranes. Our results are relevant in the context of membrane organization and show that detergents can be potent membrane reshaping agents.

MATERIALS AND METHODS

Materials

The phospholipids POPC (1-palmitoyl-2-oleoyl-*sn*-glycero-3-phosphocholine), sphingomyelin (egg, chicken), cholesterol, and the fluorescent probe Rh-DPPE (1,2-dioleoyl-*sn*-glycero-3-phosphoethanolamine-*N*-lissamine rhodamine B sulfonyl) were purchased from Avanti Polar Lipids (Birmingham, AL). Triton X-100 was from Sigma-Aldrich (St. Louis, MO). All other chemicals used were of analytical grade.

Lipid extraction from erythrocyte ghosts

Fresh human blood from healthy donors was obtained from a blood bank (approved by the Ethics in Research Committee, FCM/Unicamp, # 227/2009 protocol). Erythrocytes were isolated by centrifugation at 1000 × *g* for 5 min followed by three washes in phosphate-buffered saline (PBS, 5 mM Na-phosphate, 154.5 mM NaCl, 4.5 mM KCl, pH 7.4). After dilution of the erythrocytes in PBS (1:1, v:v), the suspension was then filtered through α-cellulose/microcrystalline cellulose to isolate erythrocytes from platelets and leukocytes (39). The purified erythrocyte suspension was then washed three times in PBS, and the packed cells were used to isolate plasma membrane (ghosts). Ghost membranes were prepared as previously described by Dodge and co-workers (40), with minor modifications (19). Briefly, one volume of packed erythrocyte cells was lysed in nine volumes of hypotonic phosphate buffer. After centrifugation, the supernatant was carefully removed and cell membranes were washed with the same buffer until white ghosts (hemoglobin-free) were obtained. Finally, the ghost membranes were washed (three times) and kept in TN buffer (25 mM Tris/HCl, 150 mM NaCl, pH 7.4). Lipid extraction from ghost membranes was performed with chloroform, methanol, and water (2:1:1, v:v:v), according to Folch's method (41). The organic phase obtained after extraction was concentrated in chloroform and phospholipids were quantified by analysis of inorganic phosphorus (42).

Preparation of GUVs

GUVs made of lipids extracted from erythrocyte ghosts and mixtures of POPC/SM/Cholesterol (2:1:2, 1:1:2 or 0.8:1:2) were grown using the electroformation method (43). Few microliters of a 2.5 mM lipid chloroform solution, with or without the fluorescent dye Rh-DPPE (1 mol % of the total lipids), were spread on the surfaces of two conductive glasses coated with fluorine tin oxide. After drying of the lipid film in a stream of N_2, the glasses were mounted to form a chamber with a 2 mm thick Teflon frame. This chamber was filled with 0.2 M sucrose solution, placed in an incubator at 50°C, and the glass slides were connected to a function generator that applied an alternating current of 1 V with a 10 Hz frequency. After 1 h, the GUVs formed were removed from the electroformation chamber and diluted ~10–20× in an equiosmolar glucose solution. The sugar asymmetry created enhanced the optical contrast of the GUVs when observed in phase contrast mode and stabilized the vesicles on the bottom of the observation chamber.

Imaging of GUVs

GUVs were observed either in phase contrast or in fluorescent mode with an inverted microscope Zeiss Axiovert 200 (Jena, Germany) equipped with a Zeiss AxioCam HSm digital camera and a 63× Ph2 objective. Fluorescence imaging was achieved with illumination from a mercury lamp HBO 103W and a set of filters with excitation at 540–552 nm and emission band at 575−640 nm. Two different experimental setups were used to observe the solubilization of GUVs by the detergent TX-100. In the first one, a 0.2 M glucose solution containing 5 mM TX-100 was injected with a glass micropipette of ~10 μm diameter placed close to a chosen GUV. The micropipettes were prepared using a vertical puller PC-10 from Narishige (Tokyo, Japan) and were controlled with a micromanipulator MP-225 from Sutter Instruments (Novato, CA). The injection flux was adjusted manually with a micrometer knob pressing a 10 μL Hamilton syringe (Sutter Instruments). In the second experimental setup, 5 μL of a suspension of GUVs prepared

in 0.2 M sucrose were diluted in 95 μL of a 0.2 M glucose solution (lipid concentration around 1 μM) containing increasing concentrations of TX-100 and then immediately placed in a homemade observation chamber. The experiments were performed either at room temperature (~22–25°C) or in an observation chamber connected to a water circulating bath to perform experiments at 37°C (the temperature was measured with a thermocouple placed inside the observation chamber).

RESULTS

The solubilization process of GUVs from erythrocyte membrane lipids (termed here as erythro-GUVs) by the detergent TX-100 was observed with phase contrast and fluorescence microscopy. A solution of 5 mM TX-100 was injected with a micropipette placed close to the selected erythro-GUVs. After contact with the detergent solution, all erythro-GUVs observed were partially solubilized, as detected by a clear decrease in vesicle size. In some cases, it was possible to clearly distinguish that part of the vesicle was first detached from the original vesicle and then completely solubilized. Fig. 1 *A* shows one such example observed under phase contrast microscopy. After 30 s of TX-100 injection, part of the erythro-GUV is detached and then solubilized in a few seconds. The last snapshot (40 s) shows the insoluble fraction of the erythro-GUV, which is clearly smaller than the original vesicle and has lost the initial sugar asymmetry responsible for the high optical contrast seen in the first snapshot. Further injection of TX-100 has no effects on the insoluble fraction. A movie of another erythro-GUV during injection of TX-100 is shown in the Supporting Material (Movie S1 *A*).

The solubilization process was also imaged with fluorescence microscopy. One selected representative sequence is shown in Fig. 1 *B*. Before contact with TX-100, all erythro-GUVs show a homogeneous distribution of the fluorescent probe used, Rh-DPPE, attesting that the lipid extract of the erythrocyte membrane did not exhibit detectable phase separation (see snapshots at 0 and 22 s in Fig. 1 *B*). The first effect caused by TX-100 was the ready formation of circular domains enriched in the fluorescent probe (as easily seen in Fig. 1 *B*, *snapshots 39–110 s*). The formed domains diffused on the vesicle surface, coalesced, and eventually the two phases were completely separated (110 s). The fact that the domains are round, diffuse, and coalesce show that both phases are liquid, i.e., *Ld* and *Lo* (44). In fact, the shape and dynamics of the domains formed in the presence of TX-100 resemble those seen in GUVs composed of classic ternary raft-like lipid mixtures, such as unsaturated PC, SM, and cholesterol, which display *Lo*/*Ld* phase separation in a certain composition and temperature range (11,12,44,45). The fluorescent probe used here is known to preferentially partition into the *Ld* phase (12,46). A control experiment showing this preferential partitioning of Rh-DPPE in the *Ld* phase was performed (see Fig. S1). Furthermore, to prove that the domains are fluid and the matrix is in the *Lo* phase, confocal microscopy images were obtained from erythro-GUVs containing the fluorescent probe Laurdan, whose emission wavelength is sensitive to the bilayer order (44) (see Fig. S2). It can be concluded that TX-100 induces the formation of detectable *Lo*/*Ld* phase separation in erythro-GUVs, in a manner similar to the commonly investigated raft-like mimetic compositions. After domain formation, the fluid part of the erythro-GUV is solubilized and the remaining insoluble vesicle—in the *Lo* phase—exhibits only a faint fluorescence (142 s). The complete movie of Fig. 1 *B* is shown in Movie S1 *B*.

The experimental design of injection with a micropipette has the drawback that the concentration of TX-100 close to the vesicle surface is not well defined, and depends on the flux condition. Therefore, a different experimental setup was also used. A small aliquot of a suspension of erythro-GUVs was added to a solution of TX-100 of known concentration, previously prepared in the observation chamber. In this setup, the vesicles in the absence of TX-100 could not be imaged. However, the effects of TX-100 at a fixed concentration could be determined. Overall, the same behavior observed with the injection protocol of a concentrated TX-100 solution was observed when the

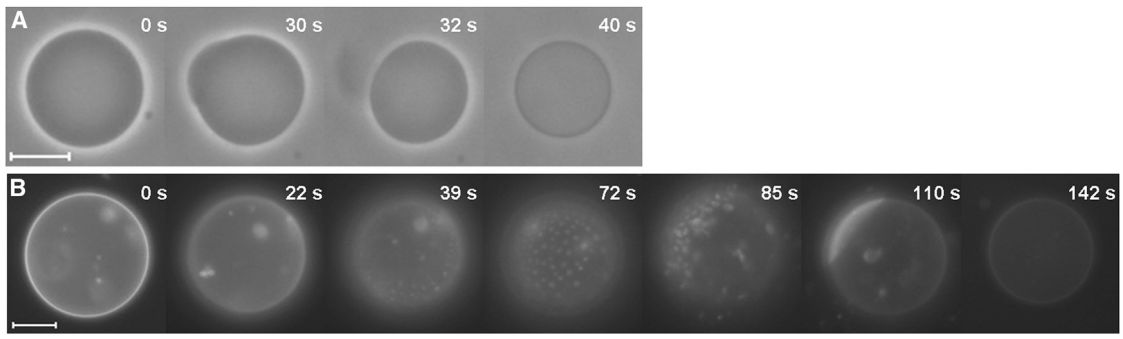

FIGURE 1 Time sequences obtained during injection of a 5 mM TX-100 solution in 0.2 M glucose with a glass micropipette close to erythro-GUVs. (*A*) Phase contrast microscopy mode, (*B*) fluorescence microscopy mode of erythro-GUVs containing 1 mol % Rh-DPPE. The indicated times refer to the moment when the vesicles were placed in front of the injection flux, which came from the right side. The scale bars represent 10 μm. Experiments were performed at room temperature. Video sequences can be seen in Movie S1, *A* and *B*.

erythro-GUVs were added to a concentration of TX-100 above its critical micelle concentration (cmc = 0.27 mM for the conditions explored here (28)). Fig. 2 shows time sequences obtained for erythro-GUVs when added to TX-100 at increasing (0.2–0.4 mM) concentrations. The complete movies of the sequences shown in Fig. 2 are shown in Movie S2, *A*, *B*, and *C*. When exposed to 0.2 mM TX-100, most of the erythro-GUVs displayed phase separation after a few seconds. Fig. 2 *A* shows that formation and coalescence of domains induced by 0.2 mM TX-100 took place within a few minutes in one erythro-GUV. In the first seconds, the vesicle surface shows a homogeneous distribution of the fluorescent probe; after 30 s *Lo*/*Ld* phase separation is promoted and the domains coalesce with time. Even after longer periods of observation (up to 10 min), only vesicles with domains were observed, but no partial solubilization. When added to 0.3 mM TX-100, thus close to the cmc of TX-100, erythro-GUVs initially show the formation and coalescence of domains within the first seconds, followed by detachment of fluid domains, as shown in Fig. 2 *B* (145–205 s). Apparently, each *Ld* patch removed reseals into one vesicle. Some of these fluid vesicles are then solubilized and the original vesicle is left with a very faint fluorescence (205 s). Addition of erythro-GUVs to 0.4 mM TX-100 causes almost immediate formation and coalescence of domains with further detachment and solubilization of the fluid part, as shown in Fig. 2 *C*. Again, each detached domain forms one vesicle that is later solubilized. After a few minutes, only the insoluble *Lo* fraction is observed (see *last snapshot* in Fig. 2 *C*). In the presence of higher TX-100 the effects observed are mainly the same as those with 0.4 mM TX-100, but the whole process occurs faster. Therefore, the onset of the partial solubilization occurs around the cmc of TX-100, in accordance with previous results on the solubilization of GUVs composed of POPC (28). At low concentrations of TX-100 (Fig. 2 *A*), only *Lo*/*Ld* phase separation is promoted. Remarkably, no change in vesicle size was observed in this initial stage, contrary to the clear increase in the size of GUVs composed of POPC (28), indicating that the insertion of TX-100 into the erythro-GUVs membrane is less favored than in fluid POPC vesicles.

The lipid extract of erythrocyte membranes comprise several lipid types with a well-known composition (47). In an attempt to model such a complex system, a predetermined ternary mixture of lipids was also investigated. Based on typical values of the relative fraction of such lipids in erythrocyte membranes (47), the ternary lipid composition 2:1:2 POPC/SM/chol (molar ratio) was chosen. GUVs of this biomimetic composition were grown and their solubilization by TX-100 was tracked with optical microscopy. Interestingly, the solubilization process of biomimetic GUVs followed the same sequence of events described previously for erythro-GUVs. One example is shown in Fig. 3 *A*. The biomimetic GUV is initially homogeneously fluorescent (0 s), showing that no detectable phase

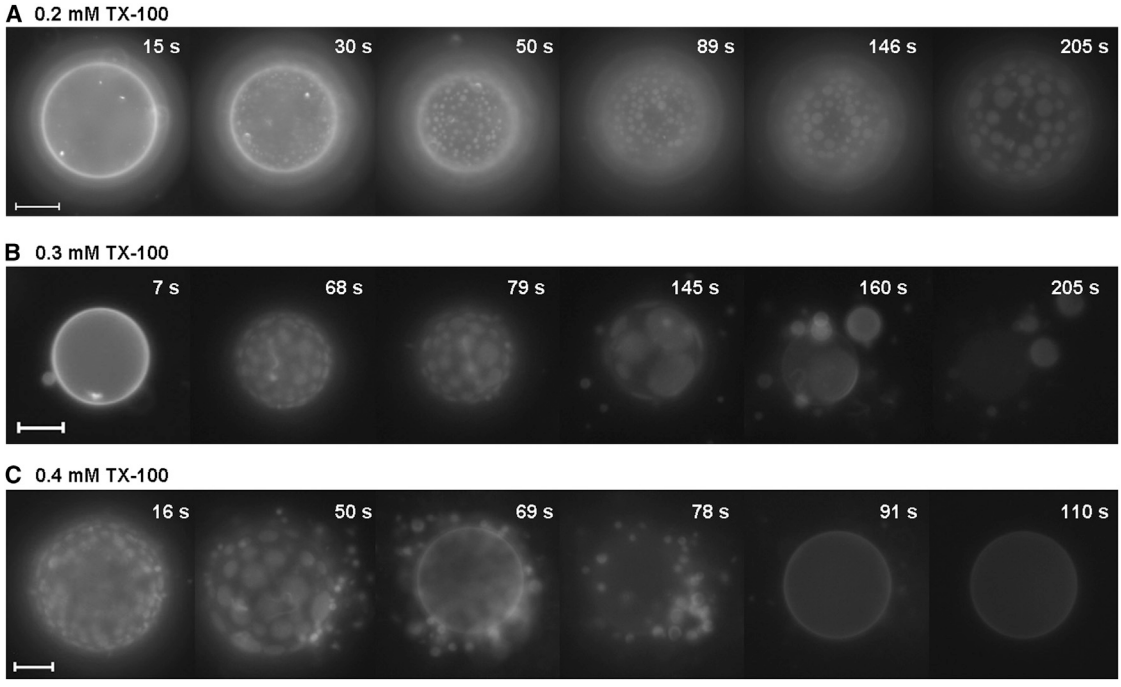

FIGURE 2 Time sequences obtained with fluorescence microscopy after addition of small aliquots of an erythro-GUVs (with 1 mol % Rh-DPPE) suspension into different concentrations of TX-100, as indicated. The indicated times refer to the moment of erythro-GUVs addition to a given TX-100 preparation. Scale bars represent 20 μm (*A*) and 10 μm (*B* and *C*). Experiments were performed at room temperature. The video sequences are shown in Movie S2, *A*, *B*, and *C*.

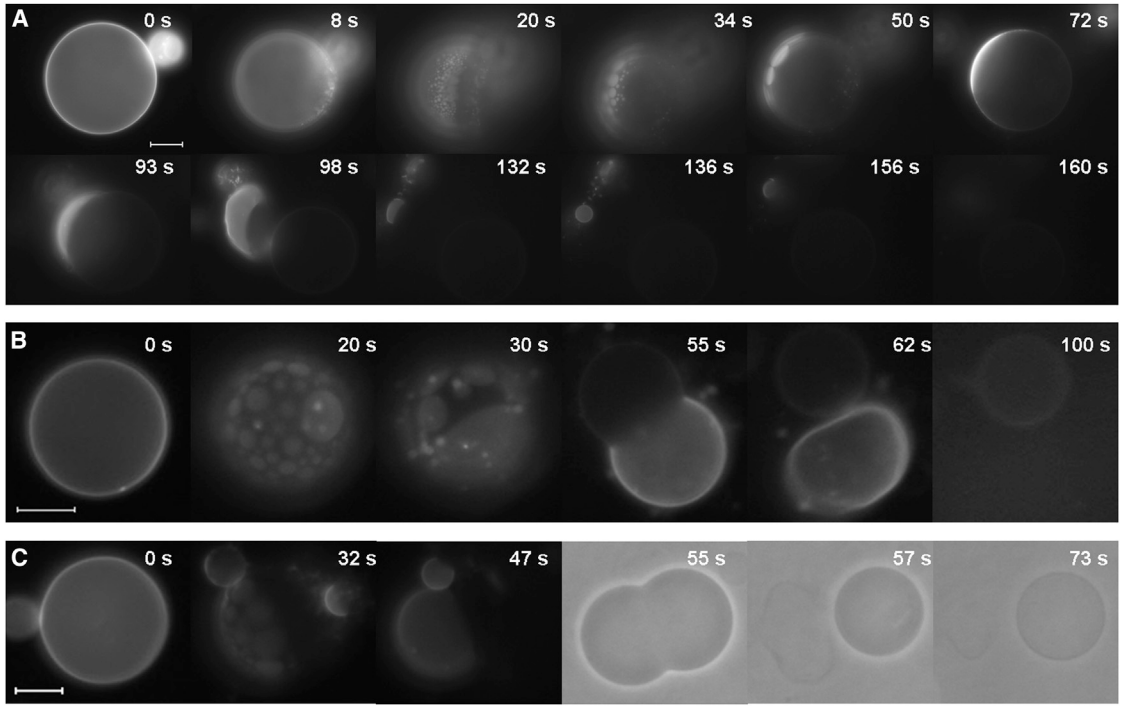

FIGURE 3 Time sequences obtained during injection of a 5 mM TX-100 solution in 0.2 M glucose with a glass micropipette. (*A*) Fluorescence microscopy of a GUV composed of 2:1:2 POPC/SM/chol at room temperature. The brightness of the last snapshot (160 s) was increased to help visualization of the insoluble vesicle fraction, which is only faintly fluorescent. (*B*) Fluorescence microscopy sequence of an erythro-GUV at 37°C. The brightness of the last snapshot (100 s) was increased to help visualization of the insoluble vesicle fraction, which is only faintly fluorescent. (*C*) Fluorescence (0–47 s) and phase contrast microscopy (55–73 s) sequence of a GUV composed of 2:1:2 POPC/SM/chol at 37°C. The indicated times on each sequence refer to the moment when the vesicles were placed in front of the injection flux, which came from the right side. The scale bars represent (*A*) 20 μm and (*B* and *C*) 10 μm. All GUVs contained 1 mol % Rh-DPPE. The respective video sequences are shown in Movie S3, *A*, *B*, and *C*.

separation is observed for this composition at room temperature. Contact with TX-100 readily promotes phase separation and domain coalescence (8–72 s). Because the injection flux comes from the right side, domains form initially on the vesicle side facing the flux, and then migrate along the vesicle surface until the *Ld* domain separates from the original vesicle (98 s) giving rise to an individual vesicle (136 s), which is then completely solubilized (160 s). The insoluble fraction that remains after 160 s is in the *Lo* phase, is clearly smaller than the initial vesicle, and only faintly fluorescent. The complete video of Fig. 3 *A* can be seen in Movie S3 *A*.

The experiments reported here were performed at room temperature. The composition of DRMs was found to be sensitive to the temperature (48), but solubilization protocols to yield DRMs are generally performed at 4°C (15,49,50). So far, only a few studies have been conducted at physiological temperature, especially for erythrocytes (16). Here, we explore the effect of increasing the temperature to physiological condition, 37°C. It would be certainly interesting to test 4°C as well, but water condensation on the chamber glass hinders optical observation below ~18°C. Basically, the same chain of events reported before at room temperature (Figs. 1 and 2) are observed for both erythro-GUVs and biomimetic GUVs at physiological temperature: the initially homogeneous membrane exhibit phase separation after contact with TX-100 and the fluid domains are detached from the original vesicle and completely solubilized. Fig. 3, *B* and *C*, show one typical erythro-GUV and one biomimetic GUV at 37°C during injection of 5 mM TX-100. The video sequences can be seen in Movie S3, *B* and *C*). It is important to stress that also at physiological temperature, erythrocyte membrane lipids and its biomimetic composition are apparently homogenous but display phase separation triggered by the presence of TX-100. The fluid fraction for both erythro-GUVs and biomimetic composition, and therefore the solubilized portion later, is clearly larger than at room temperature (compare *snapshots at 55 s* in Fig. 3, *B* and *C*, with *snapshots at room temperature*, *93 s* in Fig. 3 *A*). This was expected, as membrane fluidity should increase with temperature, especially if the melting temperature of sphingomyelins, around 40°C, is approached.

After contact with TX-100, both erythro-GUVs and biomimetic GUVs were partially solubilized, leaving a smaller insoluble spherical vesicle. The fraction of the original vesicle surface insoluble to TX-100 can be easily calculated as $X_{insoluble} = (D_{after}/D_{before})^2$, where D_{before} and D_{after} are the vesicle diameters before and after contact with TX-100, respectively. The $X_{insoluble}$ values obtained for erythro-GUVs and biomimetic GUVs at both room and

physiological temperatures are shown in Fig. 4 *A*. The $X_{insoluble}$ values obtained for erythro-GUVs at each temperature could be very well reproduced with the biomimetic composition. At room temperature, $X_{insoluble}$ for both compositions is around 0.68 ± 0.10, and this value decreases to around 0.54 ± 0.10 when the temperature is increased to 37°C. The considerably high data scatter for each membrane composition and temperature can be explained from the known variance of lipid composition within a batch of GUVs.

Based on previous and our observations (20,32,33), TX-100 selectively solubilizes the *Ld* phase only, leaving the *Lo* phase intact. Therefore, in a first approximation, we can assume that only POPC is solubilized from the biomimetic mixture (POPC/SM/chol) at room temperature, which is supported by previous data (32,33). This assumption might not hold for 37°C, because of the proximity with the melting temperature of SM. For 2:1:2 POPC/SM/chol GUVs at room temperature, around 1/3 of the vesicle surface is solubilized and 2/3 remain insoluble. Because the area per lipids in different conditions is known from previous studies, it is possible to propose a lipid composition for the insoluble fraction of this biomimetic system. The following areas per lipids were assumed here (51–53): 63 $Å^2$ for POPC in the presence of 40 mol % cholesterol (before contact with TX-100) or 70 $Å^2$ in the *Ld* phase (after contact with TX-100); 55 $Å^2$ for SM in the homogenous phase (before contact with TX-100) or 51 $Å^2$ in the *Lo* phase (after contact with TX-100); 27 $Å^2$ for cholesterol. Based on these values and our data, the proposed composition of the insoluble fraction at room temperature is 0.8:1:2 POPC/SM/chol, i.e., solubilization of 60% of the POPC lipids. To test this hypothesis, GUVs of that composition were grown and exposed to injection of 5 mM TX-100 with a micropipette. In fact, these GUVs were insensitive to the presence of TX-100, and no effects whatsoever were observed (domain formation, partial solubilization, or contrast loss). To further test the dependence of $X_{insoluble}$ on membrane composition, another composition, close to this completely insoluble one, was also probed, namely 1:1:2 POPC/SM/chol. The insoluble fraction measured for various GUVs at this composition was $X_{insoluble} = 0.91 \pm 0.07$, i.e.; between the values obtained for 2:1:2 and 0.8:1:2, as expected. Furthermore, if the same solubilization reasoning is applied for the 1:1:2 mixture, the expected composition of the insoluble fraction should also be 0.8:1:2, again validating this composition as virtually insoluble and representative of DRMs obtained at room temperature. The dependence of $X_{insoluble}$ with the membrane composition obtained at room temperature is shown in Fig. 4 *B*. Clearly, $X_{insoluble}$ increases as the relative fraction of POPC in the mixtures decreases. It would be interesting to relate the composition of the fully resistant vesicles with the composition of domains in phase separated membranes, as defined by the tie lines in the phase diagram of this system. Unfortunately, to the best of our knowledge, the phase diagram of the mixture POPC/SM/chol has not been reported, and only a few tie lines for a similar mixture have been reported so far (54).

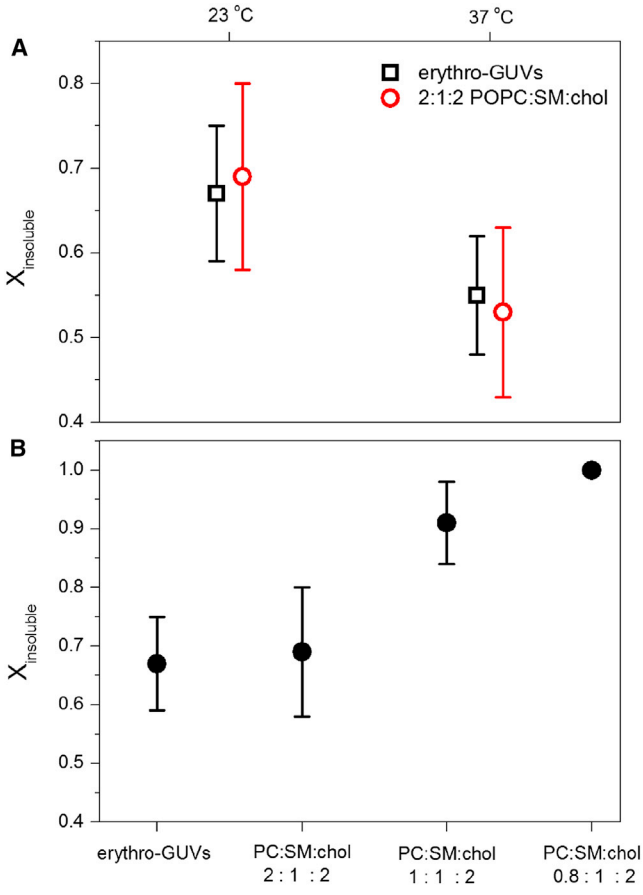

FIGURE 4 Fraction of vesicle surface area insoluble after treatment with TX-100, obtained from $X_{insoluble} = (D_{after}/D_{before})^2$, where D_{before} and D_{after} are the diameters of the vesicles before and after contact with TX-100, respectively. Only spherical vesicles were considered. (*A*) Temperature dependence of $X_{insoluble}$ of erythro-GUVs ($N = 120$ at room temperature and 51 at 37°C) and 2:1:2 POPC/SM/chol GUVs ($N = 115$ at room temperature and 20 at 37°C). (*B*) Dependence of $X_{insoluble}$ on membrane composition (indicated in the *x* axis). $N = 25$ (1:1:2 POPC/SM/chol) and 20 (1:1:0.8 POPC/SM/chol). To see this figure in color, go online.

DISCUSSION

The effects caused by TX-100 on GUVs composed of biomimetic systems of erythrocytes were observed with optical microscopy. On the one hand, the lipid extract of erythrocyte ghosts were used to grow erythro-GUVs, which retained the complexity in lipid composition of the original cells. On the other hand, a quite simple and commonly used biomimetic system was also investigated, namely 2:1:2 POPC/SM/chol. Interestingly, this simple ternary mixture could well mimic the complex biological composition of erythro-GUVs, showing that the phenomena promoted by

TX-100 in both systems arise because of fundamental physicochemical properties characteristic for simple ternary lipid mixtures. Both at room and physiological temperatures, TX-100 readily induced macroscopic *Lo*/*Ld* phase separation with further solubilization of only the fluid part, leaving insoluble a smaller vesicle in the *Lo* phase. The *Lo* insoluble fraction decreased from ~2/3 of the vesicle surface at room temperature to almost 1/2 at 37°C. Furthermore, we showed that the insoluble fraction at room temperature increases when the relative amount of POPC in the mixture is decreased, up to the point when a virtually insoluble composition, namely 0.8:1:2 POPC/SM/chol, is obtained. Our data show that both membrane composition and temperature are crucial factors determining phase separation and the fraction of insoluble membrane. Additionally, the influence of membrane proteins in detergent resistance is likely to also play a key role, which deserves to be further investigated in future works.

The findings reported here correlate well with previous studies from the literature. Calorimetric studies on 1:1:1 POPC/SM/chol show that TX-100 induces domain formation, probably because of the preferential partitioning of TX-100 into fluid bilayers, therefore segregating *Lo* patches, enriched in SM/chol (20,55). Supported lipid bilayers of ternary mixtures of DOPC/SM/chol, which exhibit *Lo*/*Ld* phase separation were imaged with AFM in the presence of TX-100 (32,33). Both studies show that TX-100 selectively solubilizes the *Ld* phase only, leaving the *Lo* domains essentially unaltered. Furthermore, Garner and co-workers (33) showed that TX-100 promotes phase separation in mixtures that were initially homogeneous. The same effect was shown in GUVs of DOPC/DPPC/chol in the presence of TX-100 (22). Our data show the same phenomena, with the benefit that GUVs offer a better picture of the cell membrane as compared to supported bilayers and that more complex biological lipid mixtures were also investigated. Furthermore, our observations reveal an interesting mechanistic aspect of the partial solubilization: The fluid domains are first removed from the insoluble vesicle, even forming separate vesicles if the process is done slow enough, and are only then finally solubilized by TX-100. Interestingly, TX-100 also promoted similar effects on the plasma membrane of COS cells (a fibroblast-like cell line) (21). TX-100 induces a profound remodeling of the plasma membrane, with the formation of highly condensed domains enriched in cholesterol and a preferential solubilization of the fluid regions of the plasma membrane. However, these observations were done at 4°C, whereas ours were performed at both room and physiological temperatures. Moreover, TX-100 was shown to induce clustering of PIP_2 in the membrane of HEK293 cells (34). The existence of an insoluble fraction after treatment of erythro-GUVs with TX-100 at both low and physiological temperature is in very good agreement with our previous data for DRMs from intact erythrocytes (16). Additionally, not only the lipid composition of the insoluble membrane fraction might be affected by the temperature, as described here, but also raft marker proteins are more solubilized at 37°C (16).

Another study proposes that TX-100 actually promotes coalescence of preexisting nanodomains rather than formation of new domains in model membranes composed of 1:1:1 POPC/SM/chol (36). Given our optical resolution (~0.3 μm) we cannot discard this hypothesis. AFM images, which offer a better spatial resolution, show that the composition that exhibited domain formation after contact with TX-100 was initially homogenous within $<$100 nm (33). Recent studies show that domain size is modulated by thickness mismatch between the *Ld* and *Lo* phases: whereas only nanoscopic domains are detected in ternary mixtures containing only POPC, domain size increases as POPC is gradually replaced in the mixture by DOPC (56). Therefore, TX-100 could induce macroscopic domain formation by preferentially partitioning into the fluid phase and inducing membrane thinning of this phase. Additionally, calorimetric studies propose that potential preexisting domains in 1:1:1 POPC/SM/chol membranes are only marginally stable and highly responsive to small perturbations (20,55). Therefore, we can hypothesize that such ternary mixtures have the potential to exhibit phase separation as a response to different stimuli. Furthermore, experiments performed on giant plasma membrane vesicles have revealed that even in a one-phase region, micrometer-scale composition fluctuations occurred, showing that the compositions of biological membranes might be tuned to reside near miscibility critical points (6,57). In living cells, which are highly dynamic complex systems not in equilibrium, several aspects of the cell membrane would prevent the development of macroscopic phase separation, such as presence of membrane-associated proteins, constraining of the membrane surface by the underlying cytoskeleton, and active transport and signaling (6,57). On the other hand, the basic constituents for lipid-driven segregation are present in biological membranes, and given the right stimuli, functional raft domains might form transiently, accomplish their function, and disassemble eventually. Furthermore, different stimuli might trigger the formation of rafts with variable composition, which might be important to allow the cell to perform distinct tasks according to the momentary requirements. It seems clear that detergents, such as TX-100, are noticeable candidates to promote such perturbation and are able to reshape both model and cell membranes. Therefore, the composition of DRMs could be influenced by the extraction protocol used. Even though our results suggest that DRMs do not represent preexisting microdomains, the use of DRMs is still useful for separation of membrane constituents and might help predict the preference of specific proteins to raft-like environment. However, we stress the importance of defining the effects caused by the detergent used in each specific extraction condition explored, because detergents such as TX-100 might affect the lateral

distribution of both lipids and proteins. Other detergents, such as $C_{12}E_8$, also widely used in biochemical studies, have also shown preferential solubilization of the *Ld* phase (27) and particularly, $C_{12}E_8$ DRMs from erythrocytes exhibited *Lo*-like phase as well as TX-100 DRMs (16,19). The resistance of biomembranes to other detergents is currently under investigation in our laboratory.

In summary, our experiments provide a direct visualization of the action of TX-100 on GUVs of a complex biological lipid composition. TX-100 undoubtedly induces macroscopic domain formation in erythro-GUVs, with a sequence of events that was found to be reproducible in a simple ternary lipid mixture (2:1:2 POPC/SM/chol). However, whether or not TX-100 promotes the coalescence of preexisting nanodomains remains an open question. After phase separation, TX-100 selectively solubilizes the *Ld* and leaves an insoluble (smaller) vesicle in the *Lo* phase. Our results conclusively show that TX-100 has a profound restructuring effect on the lateral organization of lipids in model and complex biological membranes. Therefore, detergent extraction protocols of membrane constituents should be carefully evaluated for each system and DRMs should not be directly associated with preexisting membrane structures.

SUPPORTING MATERIAL

Two figures and eight movies are available at http://www.biophysj.org/biophysj/supplemental/S0006-3495(14)00457-3.

We are thankful to Dr. Anna Seelig for the critical reading of our manuscript and to Marcus Vinicius Buri, Edgar P. Gamero, and Helena B. Nader for the confocal microscopy images.

This work was supported by the Brazilian Research foundations: FAPESP (No. 2009/0904-1; 2012/10442-8), CNPq (No. 479993/2011-4; 472054/2011-2) and INCT-FCx. C.C.D. and B.R.C. acknowledge their fellowships from FAPESP (No. 2010/18516-5) and CAPES, respectively.

REFERENCES

1. Yeagle, P. 2012. The Structure of Cell Membranes. CRC Press, Boca Raton, FL.
2. Brown, D. A., and E. London. 1998. Functions of lipid rafts in biological membranes. *Annu. Rev. Cell. Develop. Biol.* 14:111–136.
3. Pike, L. J. 2009. The challenge of lipid rafts. *J. Lipid Res.* 50 (*Suppl*):S323–S328.
4. Hancock, J. F. 2006. Lipid rafts: contentious only from simplistic standpoints. *Nat. Rev. Mol. Cell Biol.* 7:456–462.
5. Jacobson, K., O. G. Mouritsen, and R. G. Anderson. 2007. Lipid rafts: at a crossroad between cell biology and physics. *Nat. Cell Biol.* 9:7–14.
6. Baumgart, T., A. T. Hammond, …, W. W. Webb. 2007. Large-scale fluid/fluid phase separation of proteins and lipids in giant plasma membrane vesicles. *Proc. Natl. Acad. Sci. USA.* 104:3165–3170.
7. Simons, K., and M. J. Gerl. 2010. Revitalizing membrane rafts: new tools and insights. *Nat. Rev. Mol. Cell Biol.* 11:688–699.
8. Cai, M., W. Zhao, …, H. Wang. 2012. Direct evidence of lipid rafts by in situ atomic force microscopy. *Small.* 8:1243–1250.
9. Sonnino, S., and A. Prinetti. 2013. Membrane domains and the "lipid raft" concept. *Curr. Med. Chem.* 20:4–21.
10. Veatch, S. L., and S. L. Keller. 2003. Separation of liquid phases in giant vesicles of ternary mixtures of phospholipids and cholesterol. *Biophys. J.* 85:3074–3083.
11. Korlach, J., P. Schwille, …, G. W. Feigenson. 1999. Characterization of lipid bilayer phases by confocal microscopy and fluorescence correlation spectroscopy. *Proc. Natl. Acad. Sci. USA.* 96:8461–8466.
12. Baumgart, T., S. T. Hess, and W. W. Webb. 2003. Imaging coexisting fluid domains in biomembrane models coupling curvature and line tension. *Nature.* 425:821–824.
13. Dietrich, C., L. A. Bagatolli, …, E. Gratton. 2001. Lipid rafts reconstituted in model membranes. *Biophys. J.* 80:1417–1428.
14. Sezgin, E., H. J. Kaiser, …, I. Levental. 2012. Elucidating membrane structure and protein behavior using giant plasma membrane vesicles. *Nat. Protoc.* 7:1042–1051.
15. Schuck, S., M. Honsho, …, K. Simons. 2003. Resistance of cell membranes to different detergents. *Proc. Natl. Acad. Sci. USA.* 100:5795–5800.
16. Domingues, C. C., A. Ciana, …, G. Minetti. 2010. Effect of cholesterol depletion and temperature on the isolation of detergent-resistant membranes from human erythrocytes. *J. Membr. Biol.* 234:195–205.
17. Arni, S., S. A. Keilbaugh, …, D. A. Brown. 1998. Association of GAP-43 with detergent-resistant membranes requires two palmitoylated cysteine residues. *J. Biol. Chem.* 273:28478–28485.
18. Salzer, U., and R. Prohaska. 2001. Stomatin, flotillin-1, and flotillin-2 are major integral proteins of erythrocyte lipid rafts. *Blood.* 97:1141–1143.
19. Crepaldi Domingues, C., A. Ciana, …, G. Minetti. 2009. Resistance of human erythrocyte membranes to Triton X-100 and $C_{12}E_8$. *J. Membr. Biol.* 227:39–48.
20. Heerklotz, H. 2002. Triton promotes domain formation in lipid raft mixtures. *Biophys. J.* 83:2693–2701.
21. Ingelmo-Torres, M., K. Gaus, …, A. Pol. 2009. Triton X-100 promotes a cholesterol-dependent condensation of the plasma membrane. *Biochem. J.* 420:373–381.
22. Muddana, H. S., H. H. Chiang, and P. J. Butler. 2012. Tuning membrane phase separation using nonlipid amphiphiles. *Biophys. J.* 102:489–497.
23. Lasch, J., J. Hoffmann, …, K. Gawrisch. 1990. Interaction of Triton X-100 and octyl glucoside with liposomal membranes at sublytic and lytic concentrations. Spectroscopic studies. *Biochim. Biophys. Acta.* 1022:171–180.
24. Jones, M. N. 1999. Surfactants in membrane solubilisation. *Int. J. Pharm.* 177:137–159.
25. Preté, P. S., C. C. Domingues, …, S. Schreier. 2011. Multiple stages of detergent-erythrocyte membrane interaction—a spin label study. *Biochim. Biophys. Acta.* 1808:164–170.
26. Heerklotz, H., and J. Seelig. 2000. Correlation of membrane/water partition coefficients of detergents with the critical micelle concentration. *Biophys. J.* 78:2435–2440.
27. Sáez-Cirión, A., A. Alonso, …, E. A. Rivas. 2000. Equilibrium and kinetic studies of the solubilization of phospholipid-cholesterol bilayers by C12E8. *Langmuir.* 16:960–968.
28. Sudbrack, T. P., N. L. Archilha, …, K. A. Riske. 2011. Observing the solubilization of lipid bilayers by detergents with optical microscopy of GUVs. *J. Phys. Chem. B.* 115:269–277.
29. Lichtenberg, D., H. Ahyayauch, and F. M. Goñi. 2013. The mechanism of detergent solubilization of lipid bilayers. *Biophys. J.* 105:289–299.
30. Tsamaloukas, A., H. Szadkowska, and H. Heerklotz. 2006. Nonideal mixing in multicomponent lipid/detergent systems. *J. Phys. Condens. Matter.* 18:S1125–S1138.
31. Ahyayauch, H., M. I. Collado, …, F. M. Goñi. 2012. Lipid bilayers in the gel phase become saturated by triton X-100 at lower surfactant

concentrations than those in the fluid phase. *Biophys. J.* 102:2510–2516.

32. El Kirat, K., and S. Morandat. 2007. Cholesterol modulation of membrane resistance to Triton X-100 explored by atomic force microscopy. *Biochim. Biophys. Acta.* 1768:2300–2309.
33. Garner, A. E., D. A. Smith, and N. M. Hooper. 2008. Visualization of detergent solubilization of membranes: implications for the isolation of rafts. *Biophys. J.* 94:1326–1340.
34. van Rheenen, J., E. M. Achame, …, K. Jalink. 2005. PIP2 signaling in lipid domains: a critical re-evaluation. *EMBO J.* 24:1664–1673.
35. Koumanov, K. S., C. Tessier, …, P. J. Quinn. 2005. Comparative lipid analysis and structure of detergent-resistant membrane raft fractions isolated from human and ruminant erythrocytes. *Arch. Biochem. Biophys.* 434:150–158.
36. Pathak, P., and E. London. 2011. Measurement of lipid nanodomain (raft) formation and size in sphingomyelin/POPC/cholesterol vesicles shows TX-100 and transmembrane helices increase domain size by coalescing preexisting nanodomains but do not induce domain formation. *Biophys. J.* 101:2417–2425.
37. Yawata, Y. 2003. Cell Membrane: The Red Blood Cell as a Model. Wiley-VCH.
38. Pantaler, E., D. Kamp, and C. W. Haest. 2000. Acceleration of phospholipid flip-flop in the erythrocyte membrane by detergents differing in polar head group and alkyl chain length. *Biochim. Biophys. Acta.* 1509:397–408.
39. Beutler, E., C. West, and K. G. Blume. 1976. The removal of leukocytes and platelets from whole blood. *J. Lab. Clin. Med.* 88:328–333.
40. Dodge, J. T., C. Mitchell, and D. J. Hanahan. 1963. The preparation and chemical characteristics of hemoglobin-free ghosts of human erythrocytes. *Arch. Biochem. Biophys.* 100:119–130.
41. Folch, J., M. Lees, and G. H. Sloane Stanley. 1957. A simple method for the isolation and purification of total lipides from animal tissues. *J. Biol. Chem.* 226:497–509.
42. Chen, P. S., J. T. Y. Toribara, and H. Warner. 1956. Microdetermination of phosphorus. *Anal. Chem.* 28:1756–1758.
43. Angelova, M. I., and D. S. Dimitrov. 1986. Liposome electroformation. *Faraday Discuss. Chem. Soc.* 81:301–311.
44. Bagatolli, L. A. 2006. To see or not to see: lateral organization of biological membranes and fluorescence microscopy. *Biochim. Biophys. Acta.* 1758:1541–1556.
45. Kahya, N., D. Scherfeld, …, P. Schwille. 2003. Probing lipid mobility of raft-exhibiting model membranes by fluorescence correlation spectroscopy. *J. Biol. Chem.* 278:28109–28115.
46. Bagatolli, L. A. 2003. Direct observation of lipid domains in free standing bilayers: from simple to complex lipid mixtures. *Chem. Phys. Lipids.* 122:137–145.
47. Leidl, K., G. Liebisch, …, G. Schmitz. 2008. Mass spectrometric analysis of lipid species of human circulating blood cells. *Biochim. Biophys. Acta.* 1781:655–664.
48. Brown, D. A., and J. K. Rose. 1992. Sorting of GPI-anchored proteins to glycolipid-enriched membrane subdomains during transport to the apical cell surface. *Cell.* 68:533–544.
49. Pike, L. J. 2004. Lipid rafts: heterogeneity on the high seas. *Biochem. J.* 378:281–292.
50. Delaunay, J. L., M. Breton, …, M. Maurice. 2008. Differential solubilization of inner plasma membrane leaflet components by Lubrol WX and Triton X-100. *Biochim. Biophys. Acta.* 1778:105–112.
51. Maulik, P. R., P. K. Sripada, and G. G. Shipley. 1991. Structure and thermotropic properties of hydrated N-stearoyl sphingomyelin bilayer membranes. *Biochim. Biophys. Acta.* 1062:211–219.
52. Hofsäss, C., E. Lindahl, and O. Edholm. 2003. Molecular dynamics simulations of phospholipid bilayers with cholesterol. *Biophys. J.* 84:2192–2206.
53. Bezlyepkina, N., R. S. Gracià, …, R. Dimova. 2013. Phase diagram and tie-line determination for the ternary mixture DOPC/eSM/cholesterol. *Biophys. J.* 104:1456–1464.
54. de Almeida, R. F., A. Fedorov, and M. Prieto. 2003. Sphingomyelin/phosphatidylcholine/cholesterol phase diagram: boundaries and composition of lipid rafts. *Biophys. J.* 85:2406–2416.
55. Heerklotz, H., H. Szadkowska, …, J. Seelig. 2003. The sensitivity of lipid domains to small perturbations demonstrated by the effect of Triton. *J. Mol. Biol.* 329:793–799.
56. Heberle, F. A., R. S. Petruzielo, …, J. Katsaras. 2013. Bilayer thickness mismatch controls domain size in model membranes. *J. Am. Chem. Soc.* 135:6853–6859.
57. Veatch, S. L., P. Cicuta, …, B. Baird. 2008. Critical fluctuations in plasma membrane vesicles. *ACS Chem. Biol.* 3:287–293.